This article has been accepted for publication in a future issue of this journal, but has not been fully edited. Content may change prior to final publication. Citation information: DOI10.1109/TMECH.2022.3183689, IEEE Transactions on Mechatronics

Novel reconfigurable walking machine tool enables symmetric and non-symmetric walking configurations

Josue Camacho-Arreguin, Mingfeng Wang, Matteo Russo, Xin Dong, Dragos Axinte*

***Abstract*—Current research on walking robots strives to achieve a higher efficiency, a better load capacity and an increased adaptability. Parallel Kinematic Manipulators (PKMs) represent an opportunity in the search for advanced systems with higher adaptability and load capabilities. However, conventional PKMs present fixed configurations, which limit those advantages to operations within known structured environments. In this paper, a Reconfigurable Parallel Walking Machine Tool capable of adapting its configuration and gaits to walk in different scenarios is proposed. A light weight and compact repositioning system based on shape memory alloys is presented to achieve the reconfiguration capabilities. Furthermore, this paper presents the kinematic, stability and force analyses to determinate the optimal walking gaits for three different scenarios (with inclined slopes at different angles) and with four configurations. Finally, a set of experiments with the physical prototype are carried out to validate the proposed models. The results show that symmetric configurations present a better performance at lower ground inclinations (0.5% error), whilst asymmetric configurations can climb on slope conditions that would forbid the use of conventional PKMs (18% or 10º).**

***Index Terms*—Gait analysis, reconfigurable parallel kinematic machine, walking robot, machine tool.**

I. Introduction

Current research and development of walking robots have extensively relied on nature-inspired mechanisms (e.g. mammals, insects, reptiles) in search of more efficient, higher load capabilities and increased gait adaptability [1]. For instance, mammal-inspired walking robots can transport heavy loads at high walking speeds thanks to their vertically-configured legs [2]. Conversely, insect-inspired robots (e.g. hexapods) can traverse complicated terrains, as they can maintain three or more limbs in contact with the ground at any time, with higher stability coefficients than bipeds and quadrupeds. Thus, the number, distribution, and configuration of the legs play a crucial role in the performance of walking robots (e.g. speed, stability coefficients, actuation torque, etc.). Currently, most walking robots are based on fixed configurations that are selected according to desired environments and walking conditions, and their performance may be hindered if the ideal conditions are modified. Furthermore, industrial applications of walking robots require operational capabilities (e.g. inspection, machining, repair, etc.), that usually need of multi-degree of freedom, in addition to the already complicated task of locomotion. Hence, there is a need not only to walk to a particular location but also to manipulate end-effectors on complex geometry paths.

In terms of mechanical performance, Parallel Kinematic Machines (PKMs) have attracted the attention of researchers thanks to their high rigidity and precision, as PKMs consist of a series of links that connect and work together to adapt different postures between a moving platform and a fixed base [3]. Although the PKMs have been proved to be effective in reducing manufacturing times and improving the final product quality in industrial applications (e.g. aerospace [4], energy [5]), their inherent disadvantages, such as complex kinematics and control, reduced workspace, and dedicated environments for their operation significantly limit their applications.

Adaptive PKMs represent a possibility to overcome the current limitations of PKMs by enabling enhanced capabilities. Furthermore, adaptive PKMs can tailor to different environmental and operational requirements (e.g. walking and machining), providing a clear advantage against their conventional counterparts [6]. For example, PKMs are affected by the presence of singularities in their workspace, often constraining them to operate in small and fixed workspaces. However, in [7], the authors present an adaptive PKM capable to adapt its workspace to the task without singularities. Another example is presented in [8], where a 6-DoF PKM based quadruped robot is proposed for manufacturing as well as locomotion capabilities in large workspaces; further PKMs capable of both walking and machining are proposed in [9, 10]. However, these robots require external intervention for pose referencing (e.g. clamping pins in [8]), preventing autonomous use in unprepared environments. Conversely, the 6-DoF PKM hexapod in [11] is capable of walking in unstructured environments [12] and achieve high precision machining after an autonomous calibration [13].

Similarly to non-conventional PKMs, the performance of walking PKMs can be further enhanced by an adaptable mechanical architecture, able to change its geometrical parameters to optimize its layout to the environment [14, 15]. In terms of adaptive walking robots, in [14], an optimal

Corresponding author: Dragos Axinte
Submitted for review on 22/09/2021.
This work was supported in part by UK EPSRC project Robotics and Artificial Intelligence in Nuclear (RAIN) under grant EP/R026084/1.

The authors are with the Department of Mechanical, Materials and Manufacturing Engineering at the University of Nottingham NG7 2RD, U.K. (email: {josue.camachoarreguin; mingfeng.wang; matteo.russo; xin.dong; dragos.axinte}@nottingham.ac.uk)

methodology for a hexapod limb distribution is proposed to reduce the forces exerted on the limbs on flat terrain with tripod gaits only. Similarly, the hexapod in [16] can redistribute the points of attachment around its body to improve its stability, climbing capabilities and energy consumption. While these studies prove the superior capabilities of reconfigurable hexapods, the focus is on walking robots rather than on walking machines tools. However, by studying the influence of mechanism morphology on locomotion performance with kinematic and stability models, the intrinsic reconfigurability of these mechanisms can be exploited to optimize both walking and machining performance in a wide range of conditions.

To address these challenges this paper reports on the design and development of a Reconfigurable Walking Machine Tool (RWMT), This design (presented in Section II) is able to adopt many forms, from symmetric to highly asymmetrical configurations, requiring a dedicated modeling for the kinematics and stability analysis (Section III). Furthermore, the main advantage of the proposed RWMT is its capability to optimize its performance to enhance the speed of displacement, walking gaits and increased stability in a variety of terrain conditions (Section IV). With our proposed solution, any configuration for walking is possible to enable the safe operation of the RWMT in multiple environments with a reduced displacement error (Section V).

II. A Reconfigurable Walking Machine Tool

In this section, the novel concept of RWMT is proposed that enables, apart from complex path manipulation of end-effectors (e.g. machining), great abilities in readapting its configuration to the sites of interventions. First, the RWMT conceptual design is presented based on the reconfiguration mechanism on the moving platform. Then, the design for the reconfiguration mechanism is proposed as based on six identical shape memory alloy (SMA) actuated clutches and a close-loop rope-pulley mechanism. Finally, four typical configurations of the proposed RWMT are introduced.

A. Conceptual Design and challenges

In Fig. 1, a conceptual design of a RWMT integrating a moving platform with a repositioning mechanism for the limbs is presented as converted from the conventional G-S platform by removing the fixed base (to “free” six feet) Specifically, the moving platform is integrated with a novel repositioning mechanism which consists of six identical clutches and a close-loop rope-pulley mechanism driven by a single motor (see Fig. 1b). In each spherical-prismatic-spherical (SPS) limb, the upper S-joint is fixed with the clutch, which allows repositioning the limb layout on the moving platform (see Fig. 1c). Furthermore, in contrast to conventional PKMs, by removing the lower fixed base, together with the reconfiguring of the upper joints of the limbs, the proposed RWMT provides not only the flexibility to adapt to the intervention site with free-positioning feet, but also the advanced walking capability for challenging conditions, such as uneven surfaces constrained spaces and slopes.

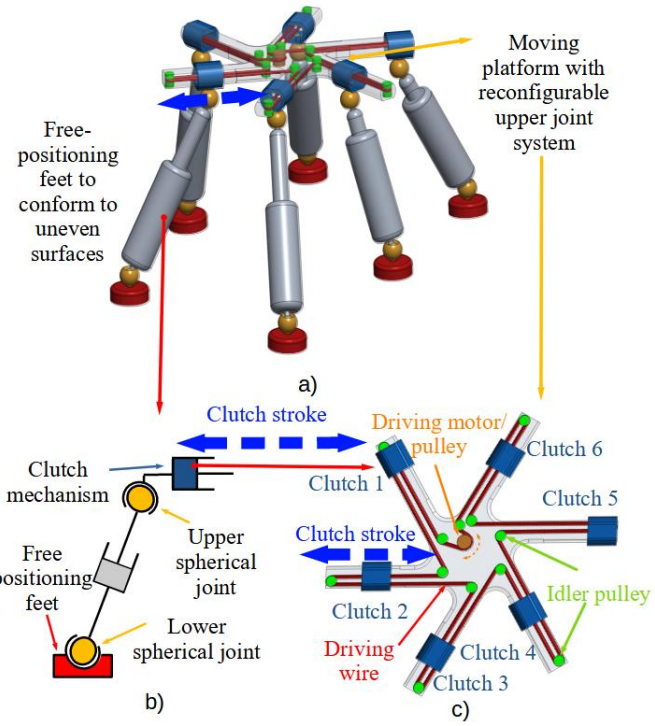

Fig. 1. Concept illustration of the proposed RWMT: a) Overview of the RWMT; b) Clutch-limb subsystem; c) Moving platform;

For a practical RWMT, three main challenges need to be addressed: 1) Optimizing the layout of clutches on the moving platform; 2) Switching the upper S-joints between passive and active modes; 3) Positioning and actuating the clutches efficiently and compactly. Furthermore, there is an increase in complexity of actuation and mass compared with conventional PKMs. First, to tackle Challenge 1, workspace and singularity analyses of the proposed RWMT have been carried out based on our previous work in [7], and a symmetric layout has been selected with each clutch positioned along the radial direction of the moving platform. Furthermore, by applying the Fourier-based methodology in [7], a new configuration can be obtained efficiently to avoid the singularities along a predefined machining path. Secondly, to address Challenge 2, a dual-mode tendon-driven upper S-joint has been adopted for the limb design from our previous work in [11], as shown in Fig. 2c. This allows each upper S-joint to switch between passive and active modes by releasing and tensioning three tendons, i.e., the S-joint is in active mode when the tendons are tensioned and in passive mode when the tendons are released.

Finally, to tackle Challenge 3, a lightweight repositioning clutch system is required, as conventional mechanisms represent heavy and bulky designs with several motors and transmission systems. Therefore, a novel repositioning system is essential for the proposed RWMT. Based on SMAs, the design of a smart actuation system is presented and will be discussed in the following subsection.

B. Smart Actuation System

SMAs are known for their capability to exert a high wrench compared to their volume [17]. This characteristic has allowed the creation of lightweight miniaturized systems incorporating SMAs in their design (when compared to electromechanical, hydraulic, and pneumatic actuators). Furthermore, successful

 This article has been accepted for publication in a future issue of this journal, but has not been fully edited. Content may change prior to final publication. Citation information: DOI10.1109/TMECH.2022.3183689, IEEE Transactions on Mechatronics

applications of SMAs in the aerospace industry [18] and medical devices [19] have shown their advantages in metamorphic and intelligent structures as compact and lightweight devices. For these reasons, SMAs are considered in this paper for the development of a novel repositioning system. Aiming to reposition six clutches individually with a single motor, a Smart Actuation System (SAS) is proposed. It consists of six identical SMA based clutch mechanisms, six linear slides, a series of pulleys, a wire-rope band, and a single motor for its actuation, as shown in Fig. 2, where:

- Each SMA-clutch mechanism is integrated with a linear slide to position its upper S-joint along the radial direction (blue dashed arrow) of the moving platform.
- A wire-rope band (red component) passes through all the SMA-clutch mechanisms and moves in two directions (red dashed arrow).
- A series of idler pulleys (green components) that guides the wire-rope band.
- A DC motor with a driving pulley (orange component). that actuates the wire-rope band.
- A knot referencing mechanism that guides the actuation limits of the wire-rope band.

The main advantage of the proposed SAS system relies on the SMA-clutches, which allow repositioning six limbs on the moving platform with a single motor. In contrast, conventional actuation packages would require a motor and its accessories (i.e. gearboxes, spindles, guides) for each limb. Thus, the smaller number of components needed for repositioning allows a lower mass on the moving platform, which is critical for a good performance of the RWMT as the inertial forces during machining and walking are significantly reduced. The two critical subsystems of the proposed SAS, the SMA-clutch and the knot referencing mechanisms, are here presented.

The novel design of the proposed SMA-clutch mechanism, as shown in Fig. 3a, is composed of a pair of shift pads, a pair of braking pads, an SMA wire, an encoder, and a linear guide. By powering on/off of the SMA wire with controlled voltage and current, the SMA-clutch mechanism is able to perform engagement (Fig. 3b) and disengagement (Fig. 3c) while moving the shift pads to release (Fig. 3b) and grasp (Fig. 3c) the running wire-rope band. Moreover, the wire-rope passes through the center of each clutch and forms a closed-loop pattern on the moving platform. Furthermore, the entire wire-rope band is actuated by a single motor, as indicated in Fig. 2a. The band movement is actuated by a single motor, which permits the actuation of the six clutches connected to each limb (simultaneously or individually), as shown in Fig. 2b. A series of test were performed to identify the correlation between the applied current and the corresponding SMA clutching force and select the optimal force. Therefore, by powering on/off the SMA wire and collaboratively actuating the wire-rope band, the proposed SMA-clutch mechanism can be utilized to displace one or more upper joint(s) of the limb along with the slide(s).

As only a single motor is required for repositioning the six limbs simultaneously or individually, the load capacity of the wire-rope band needs to be significantly higher than conventional solutions (i.e. rubber bands with payload limit of 9 N) to actuate up to six clutches simultaneously. Thus, a steel-cored wire-rope cable is selected, with the wire-rope ends clipped/knotted together to form a loop. A knot referencing mechanism is implemented to track the knot position, to prevent any blockage by the knot as shown in Fig. 3a.

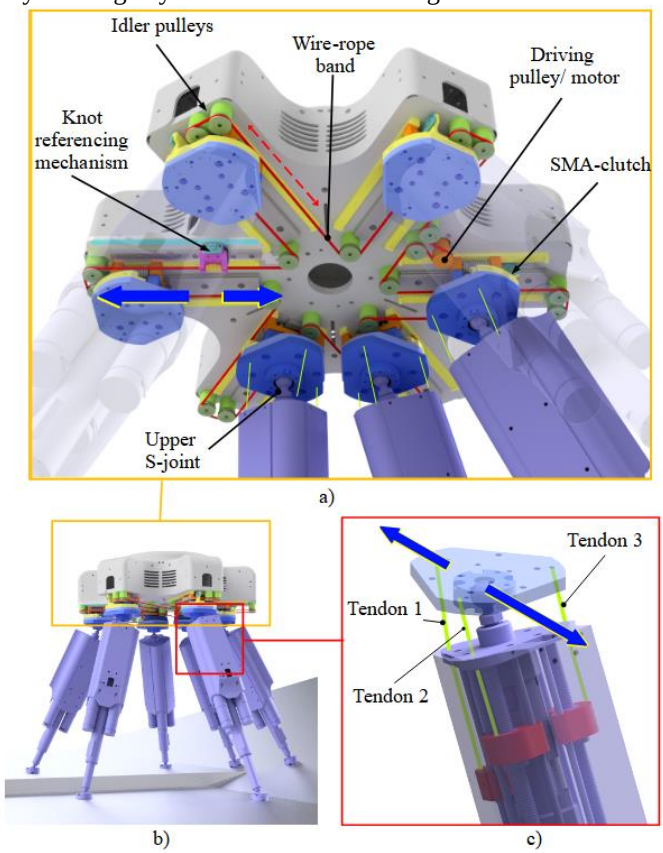

Fig. 2. Illustration of the proposed RWMT design: a) Detailed view of the SAS: a motor actuates a wire-rope band to reposition six upper S-joints; b) The RWMT over a scenario with uneven surfaces; c) Detailed view of the dual-mode tendon-driven upper S-joint.

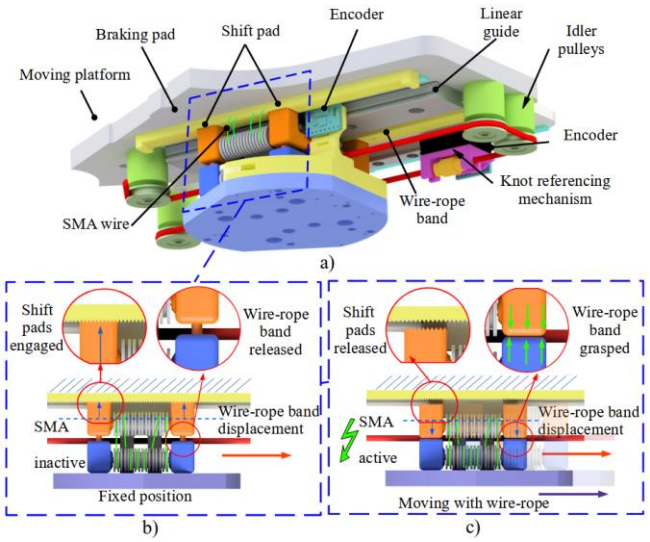

Fig. 3. Illustration of the SMA-clutch and working modes; a) Main components of the SMA-clutch; b) SMA inactive mode, the shift pads are engaged, and the position is locked; c) SMA active mode, the shift pads are disengaged, and the wire-rope band is grasped.

C. Configurations of Interest

The SAS is capable of actuating the six upper joints simultaneously or individually, which allows optimizing the configuration of the proposed RWMT for different conditions

(i.e. machining operations and walking on different terrains). This performance enhancement is due to various factors, such as singularity avoidance and optimized stiffness (when machining), and stability coefficient and speed of displacement (when walking). As shown in Fig. 4, four configurations of interest are presented as follows:

- **Insect configuration** (Fig. 4a), which arranges the upper joints aligned in two rows and limbs straight at the initial position. As the limbs maintain a quasi-vertical orientation, the feet can achieve the maximum height against the ground, and can thus avoid prominent obstacles with a rapid change in direction. Furthermore, as the limbs are lined up in two rows, the space required for walking is reduced, allowing it to pass through narrow spaces.
- **Symmetrical Hexagonal configuration** (Sym-Hex, Fig. 4b), which considers a symmetric hexagonal layout of the upper joints with the six limbs evenly distributed around the centre of the moving platform. This configuration presents the biggest support polygon, and thus the stability coefficients are the highest. However, as the limbs operate close to the maximum limits of their workspace, the maximum stride in each step is reduced.
- **G-S configuration** (Fig. 4c), which considers the same layout of upper joints in the Sym-Hex configuration, while the lower joints are arranged closer to each other in pairs. This configuration is well known in PKMs for its high accuracy and load capabilities [20]. Furthermore, compared with the Insect, this configuration achieves higher stability with an increased support polygon.
- **Asymmetrical Hexagonal configuration** (Asy-Hex, Fig. 4d), which considers an asymmetric layout of upper joints. It distributes six limbs unevenly around the centre of the moving platform, allowing to utilize more efficiently the workspace of each limb on inclined surfaces.

By reconfiguring the upper joints and removing the fixed base, two significant advantages are achieved (compared to conventional PKMs): the capability to adapt to the place of intervention and the ability to optimize its configuration between walking and machining operations. Moreover, the reconfigurability not only enhances the stiffness and singularity avoidance, as presented in our previous work [7], but also improves the stability coefficients and result in a better kinematic performance (e.g. speed, reduced displacement errors), which will be discussed in the following sections.

III. Modelling and Gait Analysis

This section presents the kinematic, stability and force analyses to determine the optimal configurations of the proposed RWMT for walking. The main advantage of the proposed models is their capability to adapt the RWMT to different terrains, in order to enhance the performance in terms of stability and displacement (i.e., speed of displacement, positioning error). To achieve this, the general kinematic model of the RWMT and its stability analysis are first developed. Then, the methodology to actuate the limbs and the force analysis for the tendons on the S-joints are presented to reduce the actuation forces by using different gaits and configurations. Finally, a comparison of the performance of different configurations for the RWMT is presented.

A. Coordinate systems

For the kinematics and stability analysis, a scheme of the proposed RWMT walking on a surface is shown in Fig. 5, where the following coordinate systems are defined:

- $\{O - XYZ\}$ represents the global coordinate system with the $-Z$-axis along the direction of gravity.
- $\{O_G - X_G Y_G Z_G\}$ represents the ground frame, where the X_G- and Y_G-axes lie on the plane defined by the ground surface. The X_G-axis is along the elevation gradient.
- $\{O_H - X_H Y_H Z_H\}$ represents the local frame fixed on the moving platform of the proposed RWMT, where O_H is at the centre of the moving platform. The X_H-axis points from O_H towards the $\boldsymbol{B_4}$, and the Y_H-axis points to the central location between the $\boldsymbol{B_5}$ and $\boldsymbol{B_6}$.
- $\{O_{B\_i} - X_{B\_i} Y_{B\_i} Z_{B\_i}\}$ represents the local coordinate system at the i^{th} upper joints, where O_{B_i} is located at the centre of the i^{th} upper S-joint (B_i), with the X_{B_i}-axis pointing towards O_H and Z_{B_i}-axis parallel to Z_H-axis. Moreover, the O_{B_i} is located on the $X_H Y_H$ plane and the distance between O_{B_i} and O_H is defined as the motion parameter c_i and controlled by the SAS.

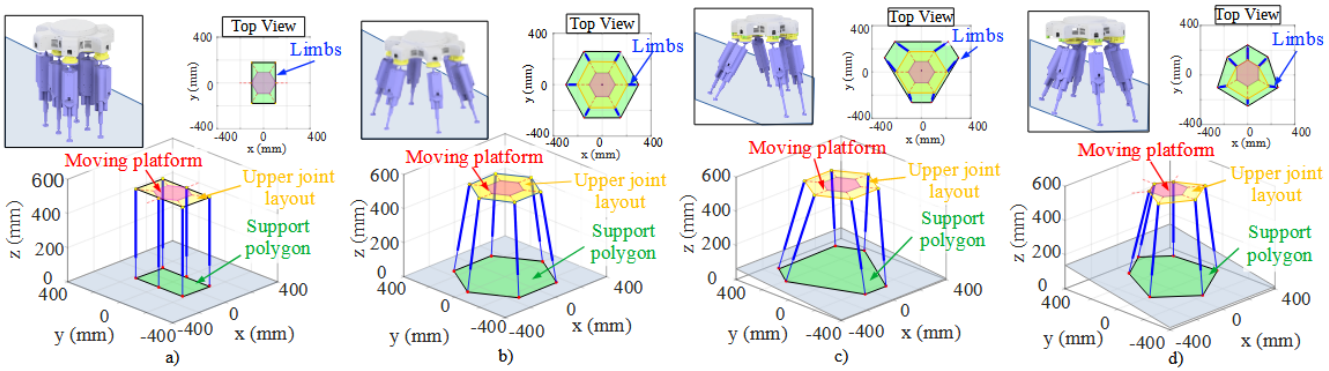

Fig. 4. Illustration of the proposed RPKWM with different configurations: a) Insect; b) Sym-Hex; c) G-S; d) Asy-Hex.

 This article has been accepted for publication in a future issue of this journal, but has not been fully edited. Content may change prior to final publication. Citation information: DOI10.1109/TMECH.2022.3183689, IEEE Transactions on Mechatronics

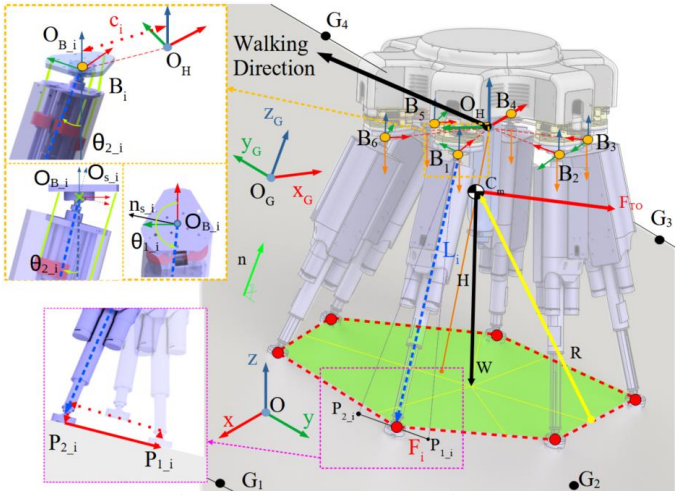

Fig. 5. Schematic of the RWMT on an inclined surface considering the pitch, yaw and roll angles for the kinematic model in the gait analysis.

B. *Kinematic and stability analysis*

This analysis starts by defining the locations that describe the plane conforming the ground. For convenience, four border points of the ground are defined in $\{O_G\}$ as:

$$^{O_G}\boldsymbol{G_k} = [x_j\ y_j\ z_j]^T \quad k = \{1,2,\dots,4\}. \tag{1}$$

Then, the position and orientation of the ground can be obtained in $\{O\}$ as:

$$^{O}\boldsymbol{G_k} = {}^{O}\boldsymbol{R}_{O_G}\,{}^{O_G}\boldsymbol{G_k} + {}^{O}\boldsymbol{O_G} \tag{2}$$

where $^{O}\boldsymbol{R}_{O_G}$ is the rotational matrix from $\{O_G\}$ to $\{O\}$ and $^{O}\boldsymbol{O_G}$ is the position of O_G in O.The relative orientation of these two frames can be defined by a rotation of $\{O_G\}$ around the Z-axis and then a rotation around the Y-axis, which defines the ground inclination against the global frame. Moreover, three ground border points $^{O}\boldsymbol{G_1}$ to $^{O}\boldsymbol{G_3}$ are used to calculate a parametric equation of the ground plane as:

$$\boldsymbol{n}\cdot\boldsymbol{P_{int}} = \boldsymbol{n}\cdot\boldsymbol{P_0} \tag{3}$$

where $\boldsymbol{n}$ is a vector normal to the ground (obtained from $^{O}\boldsymbol{G_1}$ to $^{O}\boldsymbol{G_3}$), $\boldsymbol{P_{int}}$ is a vector from $^{O}\boldsymbol{O_G}$to the points of interest on the plane, and $\boldsymbol{P_0}$ is a vector pointing from $^{O}\boldsymbol{O_G}$ to a position known on the ground. Then, to describe the O_H, $\boldsymbol{O_H}$ is defined at a distance of $|\boldsymbol{H}|$ from the ground (along with the vector $\boldsymbol{n}$, see green line in Fig. 5). It can be noted that the distance c_i is controlled by the SAS clutch mechanism which is later used to reconfigure the RWMT. The position of each upper joint can be translated from the $\{O_H\}$ to $\{O\}$ as:

$$^{O}\boldsymbol{B_i} = {}^{O}\boldsymbol{R}_{O_H}\,{}^{O_H}\boldsymbol{B_i} + {}^{O}\boldsymbol{O_H} \tag{4}$$

Nevertheless, as different angles of roll, pitch and yaw are considered for the RWMT, the distance of the upper joints from the ground can be different, leading to complex interactions between the feet and the ground in inclined ground conditions. Thus, the feet must avoid collisions and remain at a constant distance from the ground during the swing stage in the walking operation. Referring to the detailed view of the i^{th} limb in Fig. 5, further walking requirements are defined as:

- In the swing phase of the gait, the swing limbs must be lifted from the ground and swing in the direction and magnitude of the walking operation, maintaining a safe distance from the ground.
- In the support phase of the gait, all limbs must remain in contact with the ground and move backwards (from the walking direction) to produce the displacement of the platform.

A five-step procedure is proposed to model the interaction between the ground and the feet as follows:

Step 1. The neutral position of i^{th} limb from its upper joint $\boldsymbol{B_i}$ is defined to be parallel with -Z_H-axis and represented by a vector $\boldsymbol{N_{vi}}$. $\boldsymbol{P_{v,i}}$ is the intersection point between $\boldsymbol{N_{vi}}$ and the ground, which is written as:

$$\boldsymbol{P_{v,i}} = {}^{O}\boldsymbol{B_i} + t_{v,i}\boldsymbol{N_{vi}} \tag{5}$$

where $t_{v,i}$ is the coefficient defining the intersection between $\boldsymbol{N_{vi}}$ and the ground plane.

Step 2. The intersection between $\boldsymbol{P_{v,i}}$ and the ground plane is computed as a reference position for each limb. The intersection parameter $t_{v,i}$ can be obtained based on (3) and (5) as:

$$t_{v,i} = \left(\boldsymbol{n}\cdot\boldsymbol{P_0} - \boldsymbol{n}\cdot{}^{O}\boldsymbol{B_i}\right)/(\boldsymbol{n}\cdot\boldsymbol{N_{vi}}) \tag{6}$$

Step 3. $\boldsymbol{P_i}$ is computed by (7) to define the starting location of i^{th} foot on the ground with respect to the neutral position. $\boldsymbol{P_i}$ is defined at a distance A from $\boldsymbol{P_{v,i}}$ in the direction of the unit vector $\boldsymbol{N_{slide}}$. For simplicity A is a motion parameter related to the initial configuration of the RWMT and $\boldsymbol{N_{slide}}$. is defined as the vector projection of the slides on the ground.

$$\boldsymbol{P_i} = \boldsymbol{P_{v,i}} + A\,\boldsymbol{N_{slide}} \tag{7}$$

Step 4. To define the gait motion, $\boldsymbol{P_{i\_1}}$ and $\boldsymbol{P_{i\_2}}$ represents the portion of the step forward (G_F) and the portion of the step backwards (G_B) with respect to the walking direction vector $\boldsymbol{W_{Direction}}$,and are defined for each foot as lying on the ground plane and parallel to the walking direction as:

$$\boldsymbol{P_{i\_1}} = \boldsymbol{P_i} + G_F\,Step_{amp}\boldsymbol{W_{Direction}} \tag{8}$$

$$\boldsymbol{P_{i\_2}} = \boldsymbol{P_i} - G_B\,Step_{amp}\boldsymbol{W_{Direction}} \tag{9}$$

In this paper G_F and G_B correspond to half steps and assume a value of 0.5.

Step 5. The gait path is obtained as a sequence of points through an interpolation between $\boldsymbol{P_{i\_1}}$ and $\boldsymbol{P_{i\_2}}$.

Once the starting locations of the feet have been identified, the walking can be obtained by moving each limb between $\boldsymbol{P_{i_1}}$and $\boldsymbol{P_{i\_2}}$ in an iterative motion with the foot lifted during the swing from $\boldsymbol{P_{i_1}}$to $\boldsymbol{P_{i\_2}}$ and the foot on the ground in the opposite motion. To produce the displacement of the RWMT, these movements must be coordinated in groups, where one group lifts and swings the limbs to $\boldsymbol{P_{i\_2}}$ while the others support the RWMT on the ground. The proposed grouping is similar to those found in nature, as tripod gaits [21] or wave gaits [22], and their motion is optimized to avoid collisions by following the methodology in [7].

To ensure stability in the walking process, the limbs in contact with the ground must create a support polygon that contains the projection of the center of mass (CoM) of the RWMT. The position of this projection is conventionally used to compute a static stability coefficient, defined as the smallest distance of the projection to an edge of the support polygon [12, 23]. However, this criterion neglects the effect of the vertical position of the CoM, where a higher position will diminish the stability. Therefore, this paper supplements the static stability coefficient with an evaluation of the force required to tip over the RWMT ($\boldsymbol{F_{TO}}$) as expressed by:

$$\sum \boldsymbol{M_a} = (\boldsymbol{R}\times\boldsymbol{W}) + (\boldsymbol{R}\times\boldsymbol{F_{TO}}) = 0 \tag{10}$$

where $\boldsymbol{R}$ is the smallest distance from the edge of the support polygon to the CoM, $\boldsymbol{W}$ represents the weight of the RWMT.

$\boldsymbol{F_{TO}}$ represents the necessary force to maintain the static equilibrium of the RWMT and prevent the rotation of the robot around the edge of the support polygon (considering the shortest distance from the projection of the CoM). Then $\boldsymbol{F_{TO}}$ is normalized against the weight of the robot. This index is positive for stable conditions, as its value approaches zero the system is considered less stable; if the index becomes negative the system is considered as unstable. More importantly, this criterion allows a full evaluation of the stability of the RWMT in different configurations over diverse conditions for the ground (i.e., inclined ground), whereas the static stability coefficient is optimized for flat surfaces.

C. Limb actuation analysis

The limb design and actuation are based on the 3-DoF mechanism concept presented in [24]. However, to understand the influence of different configurations over the key components in the proposed RWMT, a FEA model is created in ANSYS APDL®. Based on this model, the moments required to actuate the upper S-joints and the reaction forces between the feet and ground can be obtained during different stages in the walking process, which is divided into a finite number of sub-steps. In this way, a full walking cycle can be characterized to select the most feasible configurations for walking in terms of the forces exerted on the components. To reduce the computational burden, the FEA model is defined as follows:

- The limbs are considered to perform as beam elements.
- The upper joints are connected to the centre of the platform by rigid elements.
- The mass of each component (i.e., limb and moving platform) is concentrated at its CoM.
- The supporting feet are constrained of all translational displacements.

Furthermore, to reduce the burden of the FEA analysis, the reaction forces and moments obtained from the FEA model are later used to evaluate the tensile forces on the tendons actuating each limb. As the tendons are the most critical component in the limbs, this procedure is needed to prevent excessive loading and operation failure. For this reason, a static model of the limbs is implemented by considering the moments supported by the tendons, the moments created by the weight of each limb, and the reaction forces of the feet with respect to the center of the joints, based on the results of the FEA model. The equations describing the equilibrium of each joint is:

$$\sum_{j=1}^{3} \boldsymbol{F_{i\_j}}(\boldsymbol{r_{i\_j}} \times \boldsymbol{D_{i\_j}}) + \boldsymbol{W_l}(\boldsymbol{r_w} \times \boldsymbol{g}) + (\boldsymbol{r_{f\_i}} \times \boldsymbol{R_{f\_i}}) = 0 \qquad (11)$$

where:

- $\boldsymbol{F_{i\_j}}$ is the force exerted by j^{th} tendon in the i^{th} limb.
- $\boldsymbol{r_{i\_j}}$ is a vector from the centre of the i^{th} spherical joint to the j^{th} lower tendon guide.
- $\boldsymbol{D_{i\_j}}$ *is* the vector representing the direction of the j^{th} tendon (as a unit vector) in the i^{th} limb.
- $\boldsymbol{W_l}$ is the mass of each limb.
- $\boldsymbol{r_w}$ represents the radius of action of the limb's mass.
- $\boldsymbol{g}$ is the acceleration produced by the gravity.
- $\boldsymbol{r_{f\_i}}$ is the radius of action of the reaction force of the i^{th} foot.
- $\boldsymbol{R_{f\_i}}$ is the reaction force on the i^{th} foot.

By solving (11), the forces exerted in the tendons can be computed. These results are later used to evaluate the forces in the tendons over different configurations and to select the most suitable gait types for the RWMT.

D. Walking performance analysis

As the proposed RWMT can modify its upper joint configuration, different layouts can be arranged to increase the performance of the RWMT over different walking conditions (i.e., low friction surfaces, slopes, obstacle avoidance). As presented in Section II-C, four configurations are considered in this paper: i.e., Insect, Sym-Hex, G-S and Asy-Hex, and the walking performance study of the RWMT is carried out by comparing these configurations under different terrain conditions (i.e., flat and inclined ground at 4º and 10º) with two typical gaits (i.e., wave and tripod).

The two main performance parameters are gait speed, which is directly related to the maximum step length, actuation forces, and tendon tension. As the robot performs differently when walking on flat or inclined ground, these two environments are discussed separately, and an additional stability analysis is presented for the inclined surface scenario.

The maximum step length of the robot is influenced by the height of the top platform from the ground; the physical motion limits of each actuator and components of the RWMT; the need to avoid internal and external collisions; and the stability of the system. A better capability of avoiding small obstacles on the ground could be obtained for higher platform configurations. However, higher platform configurations affect the stability of the system as reported in Fig. 6, which shows the maximum step lengths achieved by each configuration as a function of the selected platform height and summarizes the main condition limiting the maximum step size for the Insect and Sym-Hex configurations.

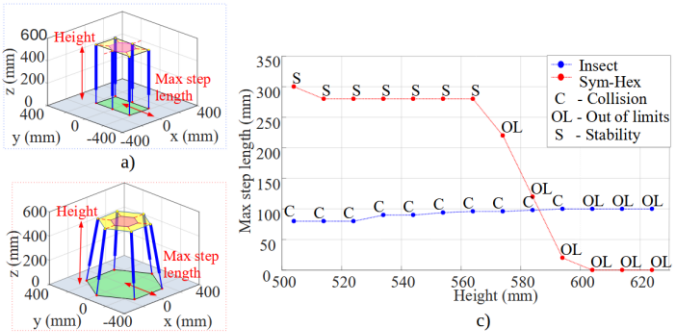

Fig. 6. Maximum step length comparison: a) Insect; b) Sym-Hex and c) Maximum step length vs platform height.

A lower but consistent maximum step length can be observed in the Insect configuration, whereas the maximum step length is significantly reduced in the Sym-Hex configuration for any height greater than 565mm. This pattern allows the Insect configuration to perform a stable walking with similar gait characteristics (e.g., step height and length) independently of the required platform height, as it can be adjusted according to the environment without a significant impact on performance.

1) Flat ground

For the flat ground scenario, the Insect and Sym-Hex configurations are selected, and the tendon forces are evaluated for the tripod and wave gaits. In the tripod gait the limbs are

 This article has been accepted for publication in a future issue of this journal, but has not been fully edited. Content may change prior to final publication. Citation information: DOI10.1109/TMECH.2022.3183689, IEEE Transactions on Mechatronics

actuated in two groups, which cycle between support and swinging in the air with a cooperative mode; in the wave gait, each limb is repositioned individually while the rest maintain contact with the ground to later effectuate the displacement of the RWMT. In both cases, the maximum load forces on the tendons are evaluated to prevent situations that could induce damage to the components, as high forces will induce larger deformations on the tendons and deviate the limbs from their ideal position. Moreover, both the Insect and Sym-Hex configurations are evaluated, and the results are summarized in Fig. *7*, which presents the maximum tensile forces exerted on the tendons of each joint and the difference of the maximum forces between the wave and tripod gaits. The comparison between gaits is based on Section III-C and is presented in Fig. *7*b and Fig. *7*d and is expressed as:

$$T_{i\_j\%} = \left(\frac{T_{Ti\_j} - T_{Wi\_j}}{T_{Wi\_j}}\right) x\ 100 \qquad (12)$$

where T_{Ti_j} and T_{Wi_j} represent the maximum tensile force on the j^{th} tendon for the i^{th} limb with the tripod and wave gaits, respectively. As per Fig. 7a, the most significant variation in forces occurs with the Sym-Hex configuration and the tripod gait, which represents an increment of up to 60% of the tendon tension force compared with the wave gait (Limb 2-T2). The maximum force found in the tendons for the Sym-Hex configuration is reduced from 119.5 N to 80 N, with the wave gait (Limb 4-T1) representing a difference of 40%. For these reasons, the wave gait is selected for the Hexagonal (symmetric and asymmetric) and G-S configurations. However, for the Insect configuration, the maximum forces exerted on the tendons are similar in both tripod and wave gait. In the Insect configuration the wave and tripod gaits can be used without significantly modifying the load conditions on the critical components of the RWMT. However, the time required to perform each displacement of the moving platform is smaller with the tripod gait. For this reason, the tripod gait is selected for the Insect configuration.

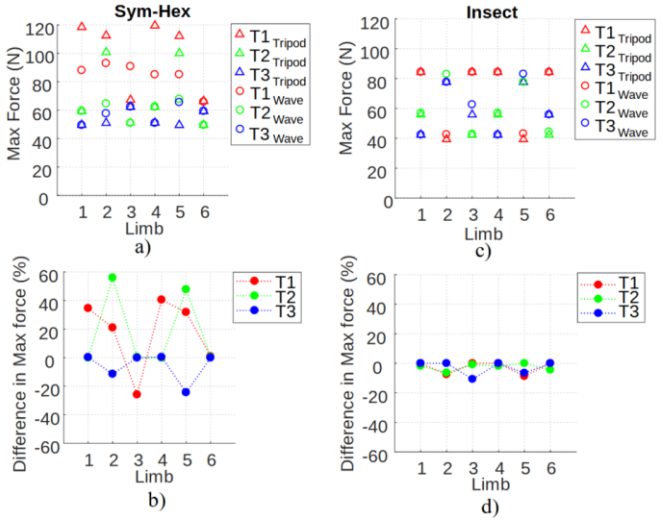

Fig. 7. Force analysis for the tendons: a) Tripod and wave gait max force for Sym-Hex; b) Difference between gaits for Sym-Hex; c) Tripod and wave gait max force for Insect; d) Difference between gaits for Insect.

2) Inclined ground

Traversing over inclined ground affects the stability of an RWMT and configurations with increased stability must be considered. As such, this section presents a study of the effects of traversing over inclined surfaces with different configurations. First, the Insect, Sym-Hex, and G-S configurations are compared considering different slope angles. Then, the effect of traversing inclined ground with different pitch angles is discussed. Finally, the Asy-Hex configuration is proposed to traverse over higher slope angles.

The analysis begins by analyzing the Insect, Sym-Hex, and G-S configurations, considering an increment from 0º to 10º of the ground inclination (i.e., the angle formed between the X_g and the plane formed by *XY*-axis). For this analysis, the moving platform is assumed to be parallel to the inclined ground, constraining the normal vector of the ground $\boldsymbol{n}$ to be parallel to the Z_H-axis. The results of this analysis are presented in Fig. 8, which shows that the stability coefficients of the Insect configuration remain stable and close to constant. However, when compared against the G-S and Sym-Hex configurations, it can be noted that the last two presents higher stability coefficients (approximately three times of the Insect). More importantly, the reduced stability coefficients of the Insect configuration could lead to unstable conditions while traversing inclined ground and thus damaging the RWMT. For these reasons, the rest of this section focuses on the G-S and Hexagonal configurations only over inclined surfaces.

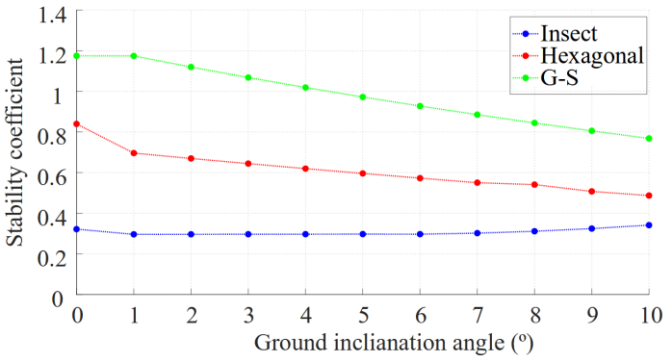

Fig. 8. Stability coefficients between 0º and 10º of inclination for the ground inclination (the platform is considered parallel to the inclined surface).

First, the effect of the pitch angle (defined as the angle formed between the Z_H axis and the *XY* plane) of the RWMT and the ground angle over the stability coefficients are analyzed. Changing the relative angle between $\boldsymbol{n}$ and the Z_H-axis of the RWMT affects the relative location of the CoM against the support polygon and thus its stability coefficients. For this study, the ground is considered to change its inclination from 0º to 10º (i.e., angle between $\boldsymbol{n}$ and *XY* plane). Similarly, the pitch angle of the RWMT is changed between 0º to 10º (i.e. angle between $\boldsymbol{n}$ and Z_H-axis). By studying the relative angle between the platform and the ground inclination, the best configuration can be chosen to traverse over different terrains. Fig. 9 presents the results of computing the stability coefficients for the G-S and the Sym-Hex configurations. Fig. 9a and Fig. 9b show that increasing the ground inclination while maintaining the platform parallel to the ground (i.e., the angles between the RWMT platform and the ground increase evenly) negatively affects the stability coefficients. Negative angles

have been considered, but this also negatively affects the stability coefficients and reduces the usable workspace of each limb, which is at its maximum when the moving platform is parallel to the ground (Z_H and Z_G are parallel). The maximum stability coefficients are obtained at a platform pitch of 0º, when the Z_H- and the Z-axes are parallel. These results consider the locations of the upper joints to be symmetrical in the G-S and Sym-Hex configurations, with all the joints on the upper platform at the same radial distance from O_H. However, these configurations are not optimal for the reachable workspace, at its maximum when the Z_H- and Z_G-axes are not parallel.

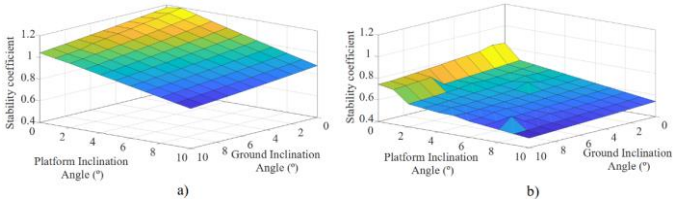

Fig. 9. Case study for the optimal attitude of the RWMT. Variation of the stability coefficients considering different platform pitch and ground inclinations. a) G-S configuration; b) Sym-Hex configuration.

Further conditions are imposed over high inclinations:

- The frontal limbs operate at the top of the workspace of each limb, restricting the minimum limb length (Fig. 10, red rectangle).
- The rear limbs operate at the bottom of the workspace of each limb, restricting the maximum limb length (Fig. 10, yellow rectangle).

These constraints would limit conventional PKMs to operate in Hexagonal and G-S configurations even at lower slope angles. However, as the upper joints are repositionable, the joints on the moving platform can be reconfigured to increase the maximum ground inclination that the RWMT can traverse.

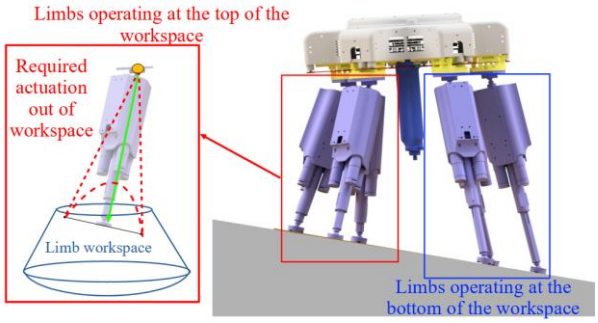

Fig. 10. Illustration of the RWMT operating at a highly inclined surface. The frontal limbs work at the top of the workspace, while the rear limbs operate at the bottom of the workspace, limiting the displacement of the RWMT.

Overall, in this section the performance of a new concept of RWMT has been evaluated based on an efficient methodology for the kinematic, stability and force analyses. These models permit the evaluation of the performance of the RWMT considering the reconfiguration capabilities and different terrain conditions. Furthermore, the result show that the RWMT can enhance its performance in terms of stability, walking gaits, forces exerted on the critical components and a better use of the workspace of each limb, by making use of its reconfigurable capabilities, as shown in Fig 11. These results are validated in the next section in a set of experiments with a RWMT prototype walking in different terrain conditions.

IV. Experimental Tests and Results

In this section, to validate the modeling and gait analysis in Section III, a prototype of the proposed RWMT has been built and tested. A VICON® motion capture system with four Vantage cameras was used to measure the movement of the RWMT. Three and five reflective markers have been added to the upper platform and to each lower joint, respectively, in order to track the poses of feet and upper platform for the evaluation of the walking performance.

First, the Insect and Sym-Hex configurations were tested with two gait types: tripod and wave. These two configurations with their ideal displacements were compared against the motion recorded by the tracking system. Then, the G-S and the Sym-Hex configurations were compared in displacement on an inclined terrain at 4º. Finally, non-symmetrical layouts of the G-S and Hexagonal configurations are reported for traversing an inclined terrain at 10º, in order to highlight the adaptability characteristics of RWMT in traversing different terrains.

A. Gait selection for the different configurations

The first comparison tested the tripod and wave gaits for the Insect and Sym-Hex configurations. When the proposed gait types (tripod and wave) were tested, the tripod gait failed in the Sym-Hex configuration in each test, as the load on the tendons increased critically when three limbs were lifted from the ground (as shown in Section III-D1.) and resulted in a significant motion error. However, the wave gait was successfully implemented in the Sym-Hex configuration. Conversely, the Insect configuration achieved tripod and wave gaits as the forces on the tendons are reduced compared to the Sym-Hex (shown in Section III-D1). This not only shows a more stable load pattern in the tendons with the Insect configuration, but also means that a longer operational life can be expected from the tendons actuating each joint, further preventing a possible failure during its walking operations.

Once the appropriated gaits were selected for each configuration, the capability to traverse over different terrains was evaluated. Three test terrains are proposed: flat ground and inclined grounds at 4º and 10º.

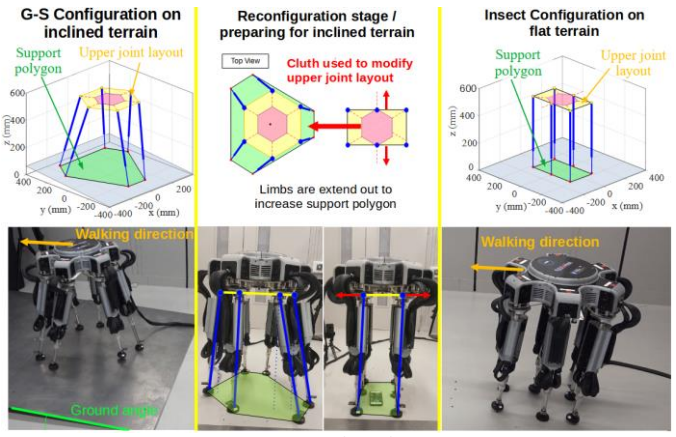

Fig. 11. RWMT enhancing its stability from flat terrain to inclined terrain. The RWMT increases is support polygon by reconfiguring the position of the upper joints and lower joints to safely traverse over inclined terrain.

 This article has been accepted for publication in a future issue of this journal, but has not been fully edited. Content may change prior to final publication. Citation information: DOI10.1109/TMECH.2022.3183689, IEEE Transactions on Mechatronics

B. *Flat ground*

The Insect and Sym-Hex configurations were proposed to test the motion capabilities of the proposed RWMT, defined as the time required to traverse the same distance and the comparison between the desired displacements against the real ones. Fig. 12 presents the results obtained during the walking of both configurations at the different stages. As both configurations aim at a total displacement of 880 mm, each step is characterized by a ground displacement of 88 mm (represented as the semi-circular lines in Fig. 12a. Furthermore, the error of the displacements and deviation were evaluated at the end of each step. Fig. 12b and Fig. 12c present the displacement error, defined as the error between the desired and real magnitude of displacement, and the direction error, defined as the error between the desired and real displacement direction, for both configurations.

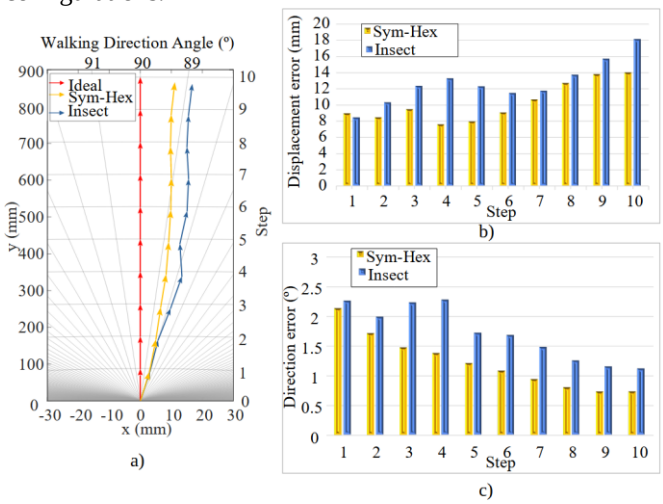

Fig. 12. Comparison between the Sym-Hex and Insect configurations. a) Displacements of the Sym-Hex and G-S configuration against the ideal displacement. b) Displacement error. c) Direction error.

The results presented in Fig. 12b and Fig. 12c show the error on each step and how these errors accumulate as the RWMT keeps moving. In both configurations, the maximum deviation error is present at the beginning of the walking, and the error value decreases at each step. The Insect configuration has the highest error at each step both in the direction of displacement and the total displacement effectuated. Nevertheless, the maximum difference between both configuration in the displacement errors of each configuration is smaller 5.72 mm and 1.14º. Furthermore, the Insect configuration completes a full step every 1.60 minutes, while the Sym-Hex performs a step every 2.94 minutes. Thus, the Insect configuration moves 1.8 times faster than the Sym-Hex configuration.

C. *Inclined ground at 4º*

The Sym-Hex and G-S configurations are selected for their increased stability coefficients when compared to the Insect configuration. The required displacement is again equal to 880 mm in 10 steps, this time performed on an inclined terrain at 4º. As shown in Fig. 13b and 13c, the maximum error is observed in the first step of the Sym-Hex configuration in both traversed distance and deviation error. Similarly, the G-S presents the maximum direction error during the first step of the walking, the maximum displacement error occurs during the last step. The deviation angles of the G-S configuration are significantly higher than those of the Sym-Hex configuration, indicating a more erratic pattern.

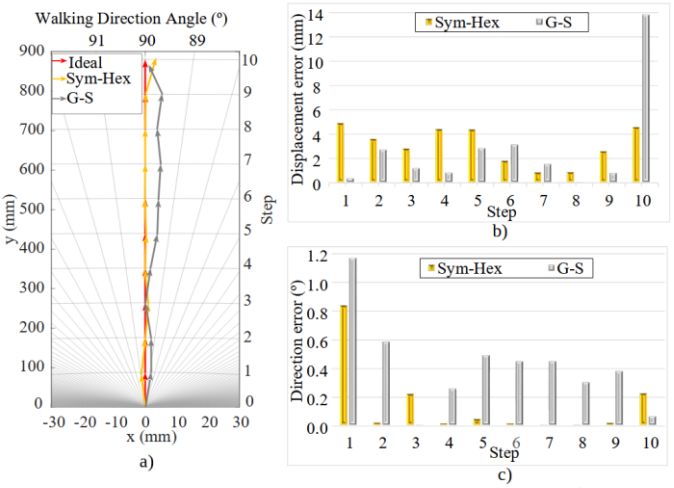

Fig. 13. Comparison between the Sym-Hex and G-S configurations. a) Displacements of the Sym-Hex and G-S configuration against the ideal displacement. b) Displacement error. c) Angular displacement error.

D. *Inclined ground at 10º*

The Sym-Hex and G-S configurations were selected for their increased stability coefficients when compared with those of the Insect configuration. However, when the ground inclination is increased, the usable workspace of each limb is reduced, as mentioned in Section III-D2. Two non-symmetrical configurations were proposed as a modification to the G-S and Sym-Hex to achieve stable displacements. In these configurations, the upper S-joints of the frontal limbs were brought closer to the center of the platform, while the ones in the rear limbs are brought to the end of the slides. The required displacement in this test is 660 mm in 10 steps, performed on an inclined ground at 10º. When the G-S configuration was tested, a considerable slippage was observed and this configuration is thus discarded. Conversely, the Asy-Hex configuration proved to be capable of displacing on inclined ground at 10º, with the results reported in Fig. 14.

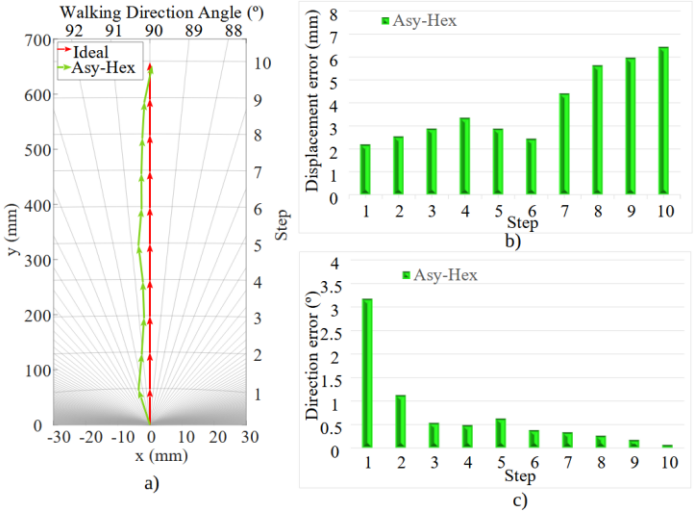

Fig. 14. Asy-Hex configuration. a) Comparison of ideal and real displacement; b) Displacement errors at each step; c) Direction errors at each step.

The Asy-Hex configuration showed a maximum displacement error at the last step with a total error of 6.42 mm. As observed in the previous tests, the maximum direction error occurs at the first step and decreases in subsequent steps.

In conclusion, the proposed RWMT has been successful in modifying its configuration to stably walk in conditions that would limit conventional parallel kinematic walking machines.

V. Discussion of Results

In the previous section, Fig. 12 presented a comparison between the Insect and Sym-Hex configurations; from Fig. 12a and Fig. 12c a higher direction error can be identified on the Insect configuration. However, the total displacement presents no significant deviation in both configurations (smaller than 5 mm). Furthermore, in Fig. 8b and Table I, a reduced stability coefficient can be observed in the Insect configuration when compared to the Hexagonal configurations, which indicates that a reduced stability coefficient can impact the total displacement performance of the RWMT. However, in these cases, the maximum deviation error remained smaller than 2º with the advantage of a higher displacement speed (1.8 times faster than the Sym-Hex, as shown in Table I). More importantly, the direction error over long distances can be solved as the Insect configuration presents the capability to displace laterally, as the Insect configuration enables changes in the walking direction of 90º with no required turning angle. Furthermore, the test also shows that the Insect configuration can avoid obstacles in the path of the RWMT (video in the supplementary material).

TABLE I
Performance Comparison of the Insect, Sym-Hex, G-S and Asy-hex Configurations

	Insect	Sym-Hex		GS	Asy-Hex.
Ground inclination (º)	0	0	4	4	10
Max displacement error (mm)	18.2	10.1	4.9	13.9	6.4
Max direction error (º)	9.6	2.4	0.8	1.2	3.2
Average displacement error (mm)	12.8	10.2	3	2.7	3.8
Min stability coefficient	0.3	0.9	0.9	1.1	0.8
Speed (step/min)	0.6	0.3	0.3	0.3	0.3

The relationship between the stability coefficient, the configuration symmetry and the error on the displacement can also be observed when the G-S and the Sym-Hex configurations are compared on an inclined ground at 4º. The Sym-Hex configuration presented a better performance in terms of direction error over the full trajectory presented in Fig. 13c and a maximal displacement error of 4.9 mm. Thus, the Sym-Hex configuration is the most suited for traversing an inclined ground, showing that more symmetrical configurations present a better performance in achieved displacement. When non-symmetrical G-S and Hexagonal configurations are compared at higher angles, slippage is seen in the G-S configuration, making it non-suitable for traversing an inclined ground at 10º. Regarding Hexagonal configurations, the symmetrical configuration shows a better performance at low inclination angles, while steeper slopes require non-symmetrical configurations for safety and to operate within the mechanical limits of the design.

In conclusion, three configurations of the RWMT are proposed to traverse different terrain conditions optimally:

- *Insect configuration:* Proposed to traverse over flat grounds when the main concern is the speed of displacement and avoiding possible obstacles.
- *Symmetric Hexagonal:* Proposed to traverse over inclined grounds when the limbs operate within allowable limits.
- *Non-Symmetric Hexagonal:* Proposed to traverse over highly inclined ground when the limbs are required to operate at their maximum actuation limits.

VI. Conclusions

This paper proposes the concept and design of a new Reconfigurable Walking Machine Tool (RWMT), which is able to:

- Modify its configuration to adopt many configurations from symmetric to no-symmetric layouts by repositioning the joints on the moving platform. This metamorphic characteristic allowed the adaptability of the RWMT to different terrain conditions, where conventional PKM would be limited. Furthermore, the proposed RWMT is lightweight and compact when the system is compared with conventional workshop machine tools, indicating the feasibility to perform in-situ operations.
- Proved the versatility of a RWMT to traverse over inclined and levelled terrain. By adopting different configurations (i.e. Sym-Hex, Insect, Gough-Stewart and Asy-Hex) different capabilities where adopted. For higher slope angles the system adopted configurations with higher stability. In conditions sucha as flat terrain the system adopted configurations that allowed higher translational speeds. Furthermore, the enhanced capabilities of the RWMT proved the versatility for in-situ repair and maintenance in environments where the terrain can vary significantly.
- Open the opportunity for the development of future portable machine tools by utilizing the reconfigurable characteristics of RWMTs, as the concept, design, kinematic models, and different configurations have been presented. Therefore, designers and researchers can use this paper as a reference for the design and analysis of RWMT.

VII. References

[1] P. Gonzalez de Santos, J. Estremera, and E. Garcia, "Optimizing Leg Distribution Around the Body in Walking Robots," *Proceedings of the 2005 IEEE International Conference on Robotics and Automation*, pp. 3207-3212, 2005.

[2] B. L. Y. Li, J. Ruan X Rong, "Research of Mammal Bionic Quadruped Robots A Review," *IEEE 5th International Conference on Robotics, Automation and Mechatronics* pp. 166-171, 2011.

[3] J.-P. Merlet, *Parallel Robots*, Second ed. ed. Springer, 2006.

[4] J. L. Olazagoitia and S. Wyatt, "New PKM Tricept T9000 and Its Application to Flexible Manufacturing at Aerospace Industry," *SAE Technical Papers*, vol. 1, 2007.

[5] S. N. Yurt, I. b. Özkol, M. O. Kaya, and C. Haciyev, "Optimization of the PD coefficient in a flight simulator control via genetic algorithms," *Aircraft Engineering and Aerospace Technology*, vol. 74, no. 2, pp. 147-153, 2002.

[6] J. Sun and J. Zhao, "An Adaptive Walking Robot With Reconfigurable Mechanisms Using Shape Morphing Joints," *IEEE Robotics and Automation Letters*, vol. 4, no. 2, pp. 724-731, 2019.

 This article has been accepted for publication in a future issue of this journal, but has not been fully edited. Content may change prior to final publication. Citation information: DOI10.1109/TMECH.2022.3183689, IEEE Transactions on Mechatronics

[7]J. Camacho, M. Wang, X. Dong, and D. Axinte, "A Novel Class of RPKM Concepts and Fourier-base Singularity Analysis " *Mechanism and Machine Theory*, vol. 153, 2020.
[8]H. Yang, S. Krut, C. Baradat, and F. Pierrot, "Locomotion approach of REMORA: A reonfigurable mobile robot for manufacturing Applications," *International Conference on Intelligent Robots and Systems*, pp. 5067-5072, 2011.
[9]N. Plitea, D. Lese, D. Pisla, and C. Vaida, "Structural design and kinematics of a new parallel reconfigurable robot," *Robotics and Computer-Integrated Manufacturing*, vol. 29, no. 1, pp. 219-235, 2013.
[10] K. S. Yang H., and Pierrot, F. , "A New Concept of Self-Reconfigurable Mobile Machining Centers," *IEEE/RSJ International Conference on Intelligent Robots and Systems*, pp. 2784-2791, 2010.
[11] D. Axinte *et al.*, "MiRoR—Miniaturized Robotic Systems for Holistic In-Situ Repair and Maintenance Works in Restrained and Hazardous Environments," *IEEE/ASME Transactions on Mechatronics*, vol. 23, no. 2, pp. 978-981, 2018.
[12] A. Rushworth, S. Cobos-Guzman, D. Axinte, and M. Raffles, "Pre-gait analysis using optimal parameters for a walking machine tool based on a free-leg hexapod structure," *Robotics and Autonomous Systems*, vol. 70, pp. 36-51, 2015.
[13] A. Olarra, D. Axinte, L. Uriarte, and R. Bueno, "Machining with the WalkingHex: A walking parallel kinematic machine tool for in situ operations," *CIRP Annals*, vol. 66, no. 1, pp. 361-364, 2017.
[14] P. Gonzalez de Santos, E. Garcia, and J. Estremera, "Improving walking-robot performances by optimizing leg distribution," *Autonomous Robots*, vol. 23, no. 4, pp. 247-258, 2007.
[15] i. h. A. K. Ozyalcin, Y. Ozturk, B. Mengus, H. Ozakyol and Z. Bingul, "New Design and Development of Reconfigurable Hybrid Hexapod Robot," *Annual Conference of the IEEE Industrial Electronics Society*, pp. 2583-2588, 2018.
[16] G. Zhong, L. Chen, and H. Deng, "A Performance Oriented Novel Design of Hexapod Robots," *IEEE/ASME Transactions on Mechatronics*, vol. 22, no. 3, pp. 1435-1443, 2017.
[17] P. Motzki, F. Khelfa, L. Zimmer, M. Schmidt, and S. Seelecke, "Design and Validation of a Reconfigurable Robotic End-Effector Based on Shape Memory Alloys," *IEEE/ASME Transactions on Mechatronics*, vol. 24, no. 1, pp. 293-303, 2019.
[18] D. Hartl, B. Volk, D. C. Lagoudas, F. Calkins, and J. Mabe, "Thermomechanical Characterization and Modeling of Ni60Ti40 SMA for Actuated Chevrons," pp. 281-290, 2006.
[19] N. Jang *et al.*, "Compact and Lightweight End-Effectors to Drive Hand-Operated Surgical Instruments for Robot-Assisted Microsurgery," *IEEE/ASME Transactions on Mechatronics*, vol. 25, no. 4, pp. 1933-1943, 2020.
[20] C. Yuan, R. Gexue, and D. ShiLiang, "Vibration control of gough-stewart platform on flexible suspension," *IEEE Transactions on Robotics and Automation*, vol. 19, no. 3, pp. 489-493, 2003.
[21] M. Wittlinger, R. Wehner, and H. Wolf, "The desert ant odometer: a stride integrator that accounts for stride length and walking speed," *J Exp Biol*, vol. 210, no. Pt 2, pp. 198-207, Jan 2007.
[22] M. Grabowska, E. Godlewska, J. Schmidt, and S. Daun-Gruhn, "Quadrupedal gaits in hexapod animals - inter-leg coordination in free-walking adult stick insects," *J Exp Biol*, vol. 215, no. Pt 24, pp. 4255-66, Dec 15 2012.
[23] A. A. F. R.B. McGhee, "On the Stability Properties of Quadruped Creeping Gaits," *Mathematical Biosciences*, vol. 3, pp. 331-351, 1968.
[24] N. Ma, J. Yu, X. Dong, and D. Axinte, "Design and stiffness analysis of a class of 2-DoF tendon driven parallel kinematics mechanism," *Mechanism and Machine Theory*, vol. 129, pp. 202-217, 2018.

Josue Camacho-Arreguin received the B.Eng. in aeronautical engineering from I.P.N, Mexico in 2013; and the M.Eng. degree in aeronautical engineering by U.A.N.L, Mexico in 2016. He is currently working towards the Ph.D. degree in mechanical engineering at the University of Nottingham, working on parallel mechanisms for in-situ repair and maintenance. His research interests are mechanical design, structural analysis and robotics.

Mingfeng Wang received the B.Eng. degree in mechanical design and automation and the M. Eng. Degree in mechanical engineering from Central South University, Changsha, China, in 2008 and 2012, respectively and the PhD degree in mechanical engineering from University of Cassino and South Latium Italy in 2016. He is currently a Research Fellow at Rolls-Royce University Technology Centre (UTC), University of Nottingham, UK. His research interests cover humanoid robots, precision farming robots, continuum robots.

Matteo Russo (M'18) received the B.Sc., M.Sc. and Ph.D. degrees in mechanical engineering from the University of Cassino, Italy, in 2013, 2015, and 2019, respectively. Between 2015 and 2017 he was a visiting researcher at RWTH Aachen University, University of the Basque Country and Tokyo Institute of Technology.

Since 2019, he is a Research Fellow at the Rolls-Royce UTC in Manufacturing and On-Wing Technology, University of Nottingham, Nottingham, UK. His main research interests are continuum robots, robot kinematics and parallel manipulators.

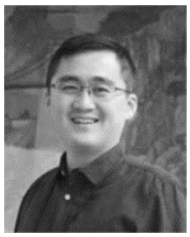

Xin Dong received his B. Eng. Degree in mechanical engineering from Dalian University of Technology, Dalian, China 2008, the M. Eng and PhD degrees in Mechatronics, Robotics and Automation Engineering from Beihang University, Beijing, China in 2011 and from University of Nottingham, Nottingham, UK, 2015.

He is currently an Assistant Professor working at the University of Nottingham. His research interests are extra slender continuum robot and reconfigurable hexapod robots with novel actuation solutions for the application in Aerospace, Nuclear, Oil & Gas, Marine and rescue.

Dragos Axinte received the M.Eng. degree in manufacturing engineering in 1988, and the Ph.D. degree in manufacturing engineering in 1996.

After graduating, he worked in R&D in industry for 10 years and then moved to academia to lead research in the field of machining, process monitoring and design of innovative tooling/robotics for in-situ repair especially related to on-wing repair of aeroengines.

Currently, he is Professor of Manufacturing Engineering at University of Nottingham and Director of Rolls-Royce University Technology Centre (UTC) in Manufacturing and On-Wing Technology.